ChemistryOpen

Research Article
doi.org/10.1002/open.202200200

Chemistry Europe
European Chemical Societies Publishing

www.chemistryopen.org

A Xanthan-Gum-Stabilized PEG-Conjugated Nanocurcumin Complex: Telescoping Synthesis for Enhanced Permeation Potential

Prem Pandey[+],[a] Supriya Chaturvedi[+],[b] Rutuja Gumathannavar,[a] Mandar M. Shirolkar,[a] Vijay Kanuru,[c] Atul Kulkarni,*[a] and Sang Hyun Moh*[d]

We report a facile room temperature telescoping synthesis of a nanocurcumin complex with 17.5-fold permeation enhancement as determined by comparative in vitro permeation study with raw curcumin. The permeation results were further validated with in silico drug absorption prediction using ADMET predictors.

Introduction

Curcumin (Curcuma longa), a turmeric plant extract, has been one of the most widely studied natural phytochemicals owing to its diverse biological properties such as being anti-inflammatory,[1] an antioxidant,[2] anti-depressant,[3] mitigating risk of heart disease,[4] showing anti-cancer properties,[5] and helping to clear amyloid plaques in Alzheimer's.[6] However, curcumin, being a polyphenol, is hydrophobic in nature,[7] has poor absorption, low drug-receptor binding activity, expeditious metabolism, and shows systemic clearance leading to curtailed bioavailability.[8] The poor bioavailability of curcumin is aggravated by the fact that it binds with enterocyte proteins which modify its structure and prevent its passive diffusion across the cell membrane.[9] These limitations have limited curcumin usage to a mere nutritional supplement despite possessing immense therapeutic potential and thus a clinical lead molecule.

Globally, researchers are working to solve the long-standing problem of oral bioavailability of phytochemicals.[10] To date, innumerable attempts have been made, including chemical complexation (curcumin-lecithin, curcumin-alginate),[11] encapsulated curcumin formulations (curcumin-PEG, curcumin-phospholipids),[12] non-symmetrical aza-aromatic curcuminoids,[2] and various nano-delivery systems (curcumin conjugates of non-steroidal anti-inflammatory drugs, curcumin-loaded PLGA-PEG nanoparticles).[5c,13] However, the use of organic solvents or unsaturated compounds to solubilize curcumin produces cytotoxic effects and may not make for ideal therapeutic candidates.[13] It is also difficult to achieve batch reproducibility during commercial curcumin–polymer complex synthesis.[14] Another study reported a 3-fold increase in stability for hyaluronic acid polymer-coated curcumin. They also reported slow release of curcumin from the complex in simulated gastrointestinal fluid, yet did not mention anything about cellular uptake.[15] Dey et al. reported the development of a curcumin-alginate conjugate using an esterification reaction to improve solubility and stability.[16] However, an ester linkage can be cleaved by acid or esterases in the stomach at acidic pH and the desired delivery to the intestine may thus not be attained.[13] Li et al. reported the controlled release of the conjugated drug camptothecin-poly(carboxybetaine) mediated by esterase in an acidic environment that resembles the acidic environment of the stomach.[17] Therefore, it is imperative to design a permeable curcumin with an appropriate chemical complex which could prove to be a potential therapeutic candidate without adverse effects.

Results and Discussion

Herein, we report a facile room-temperature telescoping emulsification process (Figure 1) of raw curcumin (RC) by selectively combining hydrophilic solubilizers PEG-400, XG and PS-80 for preparation of bioavailable nanocurcumin complex (CurNP) (See Supporting Information section 1.2 for details).

It has already been reported that particle conjugation by low molecular weight polyethylene glycol (PEG-400) is one of

[a] P. Pandey,[+] R. Gumathannavar, Dr. M. M. Shirolkar, Prof. Dr. A. Kulkarni
Symbiosis Center for Nanoscience and Nanotechnology (SCNN)
Symbiosis International (Deemed University) (SIU)
Lavale, Pune 412115, Maharashtra (India)
E-mail: atul.kulkarni@scnn.edu.in
[b] S. Chaturvedi[+]
Nuimance Phytovigyan Private Limited (NPPL)
Anusha Enclave, Pashan-Sus Road
Pune 411021, Maharashtra (India)
[c] Dr. V. Kanuru
Oncocur India Private Limited
#1, Pitruchhaya, Sanghavi Corporate Park
Govandi (E) Mumbai 400088 (India)
[d] Dr. S. H. Moh
Plant Cell Research Institute of BIO-FD&C
509-512, Smartvalley A, 30
Songdomirae-ro, Yeonsu-gu
Incheon 21990 (South Korea)
E-mail: biofdnc@gmail.com
[+] These authors contributed equally to this work.

Supporting information for this article is available on the WWW under https://doi.org/10.1002/open.202200200

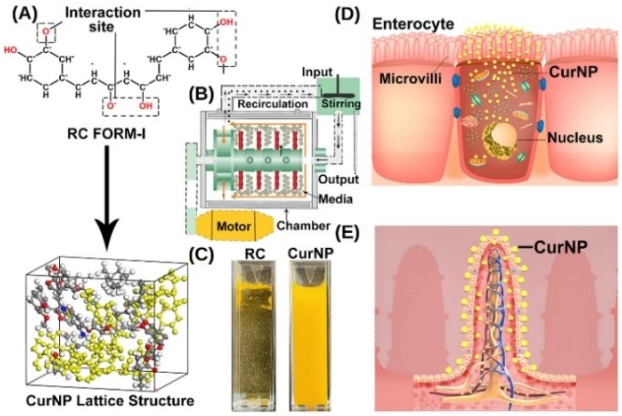

Figure 1. (A) Raw curcumin (RC) form-I structure as confirmed by X-ray powder diffraction studies and possible interaction site as illustrated with the help of DFT simulation; (B) schematic diagram of Bead mill used for CurNP nanocomplex formation. The bead mill image has been recreated and the original image was provided by Jay Instrument, Mumbai (India). (C) RC and CurNP water dispersion (actual image). (D) Representative CurNP absorption in the most abundant simple columnar epithelial cell lining of small intestine, i.e. an enterocyte (intestinal absorptive cell). (E) Intestinal villi anatomy (epithelial cells with microvilli and capillary network) demonstrating representative transport of CurNP to blood capillaries. (The standard license for the background images of Figures 1D & 1E have been obtained from Adobe Stock images).

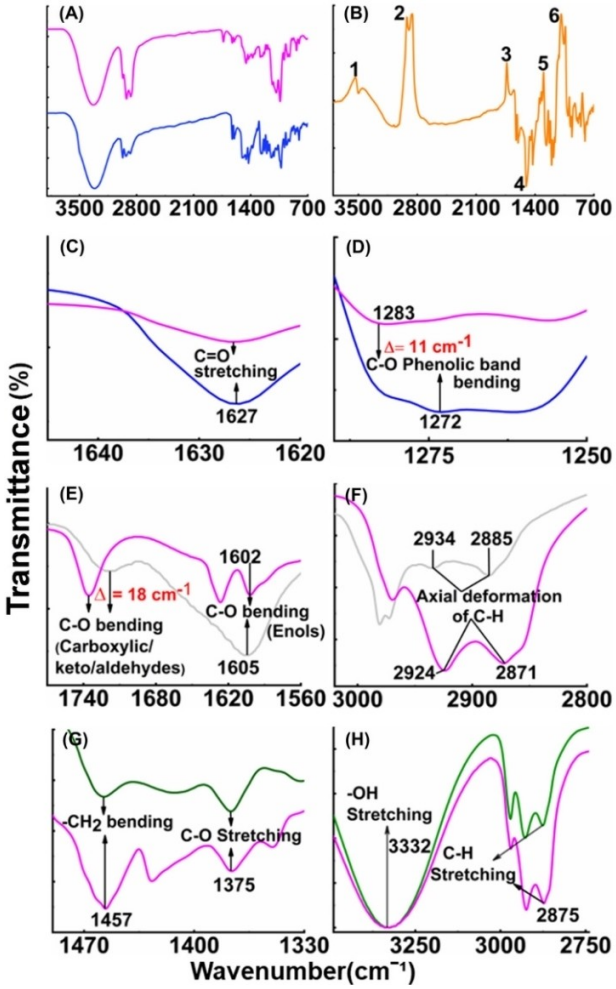

Figure 2. FTIR spectra of CurNP (magenta), RC (blue), XG (grey) and PEG400 (green). (A) Comparative spectra of CurNP & RC. (B) Transmission intensity difference plot between CurNP & RC. No. 1 & 2 demonstrate –OH group intensity, 3&4 C–O (carboxylic/keto/aldehydes) and enol group, and 5&6 the $-CH_2$ bending & C–H stretching vibration intensity difference. (C) C=O stretching at 1627 cm^{-1} for CurNP and RC. (D) C–O phenolic band bending at 1273 cm^{-1} for RC and 1284 cm^{-1} for CurNP with a blue shift of 11 cm^{-1}. (E) The CurNPs and stabilizer XG demonstrating peaks pertaining to C–O (carboxylic/keto/aldehydes) at 1736&1718 cm^{-1} (blue shift of 18 cm^{-1} for CurNP) and C–O (enols) at 1602&1605 cm^{-1}, respectively. (F) CurNP and RC show C–H bond axial deformation in the range of 2934–2871 cm^{-1} with CurNP exhibiting a slight red shift of 10 cm^{-1}. (G & H) CurNP and PEG400 demonstrate $-CH_2$ bending vibration at 1457 cm^{-1} & C–O stretching vibration at 1375 cm^{-1}, while –OH & C–H stretching vibrations are visible at 3332&2875 cm^{-1}, respectively.

the most widely used methods in medical applications. PEG chains provide a good molecular hydration layer.[18] They surround the conjugated particle by formation of a steric shield around it and reduce stereo-electronic as well as hydrophobic interactions of biomolecules to attain a stable aqueous dispersion even in an extreme range of pH conditions.[18] PEG-particle conjugation protects particles from phagocytosis, reduces liver metabolism and prolongs blood circulation.[18] In contrast, long-chain polysaccharide xanthan gum (XG), a natural polysaccharide and a dispersant, abets the non-ionic surfactant's polysorbate-80 (PS-80) ability to reduce interfacial tension of water and RC's polyphenols and steers the emulsification process.[19] Therefore, amalgamation of the above-mentioned molecules with RC could be a novel approach to prepare a potential therapeutic permeable candidate.

Interestingly, FTIR spectral analysis reveals notable difference in functional groups of RC and CurNP (Figures 2A and 2B). A detailed analysis divulges important functional groups such as enol and carbonyl groups from β-diketone moiety (Figure 2C), phenolic hydroxyl groups (Figure 2D), phenyl rings, unsaturated carbon and methoxy groups (Supporting Information, Figure S2).[20] These functional groups serve as a potential binding site, along with additional functionality provided by keto-enol tautomerism for other molecules present in the CurNP.[21] The important bands observed in CurNP at 1627 cm^{-1} (aromatic moiety C=C stretching), 1457 cm^{-1} (olefinic CH_2 bending vibrations) and 1284 cm^{-1} (C–O phenolic band bending) are the characteristic peaks of curcumin.[22] The peak shifts of 1284 from 1273 cm^{-1} (Figure 2D) and of 1736 from 1718 cm^{-1} (Figure 2E), the strengthening of the absorption peak around 3300 cm^{-1} (Figure 2A), the presence of bands in the range of 2950–2850 cm^{-1} and 1375 cm^{-1} due to absorption of symmetrical as well as asymmetrical stretching vibrations of aromatic $-CH_3$ and $-CH_2$ groups and enol C–O stretching vibrations[23] indicates the interaction of RC with XG (Figures 2E and 2F) and PEG400 (Figures 2G and 2H). The –OH stretching vibration peak with higher intensity observed at around 3300 cm^{-1} for CurNP (Figure 2A) indicates the role of the –OH group in intermolecular hydrogen bonding.[24]

This observations were further corroborated with the density functional theory (DFT)-simulated calculation of molecular electrostatic potential values (MESP).[25] The large negative values of MESP in the range of −50 to −30 kcal mol^{-1} (parrot

green colour, Figure 3A) has been attributed to the negatively charged oxygen atoms of carbonyl and hydroxyl groups (electrophilic reactive centre).[26] Similarly, the C–O bending observed at around 1736 cm^{-1} (Figure 2E) with its considerable change in frequency (Figure 2B) suggests formation of a pπ-pπ bond between carbon and oxygen atoms.[27] The observed peak shift may be due to the altered nature of carbonyl group as a result of unequal distribution of bonding electrons between two atoms and the presence of a lone pair of electrons at the oxygen atoms.[21] The shift observed at 1602 cm^{-1} is attributed to enolic C–O bending.[23a] Furthermore, the C–O stretching vibration observed at around 1375 cm^{-1} has been attributed to the primary –OH group from PEG400.[23b] The MESP-mapped van der Waals surface of simulated CurNP complex also suggests that PEG-400, XG and PS-80 selectively interact with the phenol ring of the curcumin molecule and their interaction sites exhibit large positive value of ESP within the range +20 to +70 kcal mol^{-1} (Represented with magenta colour, Figure 3A).[28] The binding energy profile further confirms that PEG-400 and XG strongly interact at values of +65 kcal mol^{-1} and +47 kcal mol^{-1}, respectively, while the hydrophilic part of PS-80 interacts with RC with an energy of −15 kcal mol^{-1} (See Supporting Information, Figure S4(B)). Thus, FTIR spectroscopy along with MESP results conclusively show the stabilization of the RC molecule through the interactions with PEG-400, XG and PS-80 for the formation of CurNP.

Notably, we prepared CurNP in aqueous medium (Figure 1C) and the dispersion stability has been corroborated with high negative zeta potential (−44.07 ± 0.54 mV) value compared to RC's (−22.24 ± 1.23 mV) less negative value (Figure 3B).[29] Interestingly, the CurNP zeta potential value is in line with the simulated surface charge density value (−45.0 mV) of CurNP (Figure 3B, inset). These trends were also evident from the zeta potential values measured over a period of 144 h for CurNP and RC (See Supporting Information, Figure S5). In order to obtain reliable dispersion stability information, the slope of the curve was obtained (See Figure S5). The higher the slope, the lower was the dispersion stability. RC showed a 50% reduction in zeta potential values during 144 h vs. CurNP (15% reduction). Thus, the above-detailed observations conclusively demonstrate the estimated enhancement (3.3-fold) of CurNP dispersion stability over RC.[29b] Interestingly, a blue shift of 49 nm in localized surface plasmon resonance (LSPR) peak of CurNP as compared with RC was observed (Figure 3C).[30] The shift may be the result of a quantum confinement effect leading to the quantization of band levels and a shift of the band gap to shorter wavelengths with reduction in particle size.[31]

The PS-80 present in the reaction mixture undergoes reorganisation, leading to change in the medium dielectric constant and subsequently resulting in the LSPR peak position shift. The reorganised PS-80 contributes to the increased dispersion stability that is evident from CurNP's zeta potential values (Figure 3B) and the DFT simulation calculations (Figure 3C, inset).[32] The DFT simulation supports the experimental LSPR observations by estimating RC (5.9 eV) to CurNP (2.80 eV) HOMO-LUMO energy gap change (See Supporting Information, Figure S7 and Table S2). This decreasing energy gap shift indicates higher molecular interaction that leads to a stable aqueous CurNP dispersion.

We performed PXRD studies on RC and CurNP (Figure 4A and Figure S3, Supporting Information). The CurNP diffraction peaks are broad when compared to RC, which evidently confirmed the conversion of RC to nano form of RC along with chemical complexes which is nothing but CurNP in our case. The Rietveld refinement of PXRD pattern of commercially available RC matches with Form 1 polymorph as reported by Sanphui et al.[33] Interestingly, the PXRD pattern of CurNP matches well with Form 1 (62.2%) as well as with Form 2 (37.7%) which indicates a composite form of CurNP (See Supporting Information Table S1 for detailed structural parameters and % calculation). Thus, the above observations suggest that the prepared CurNP complex has high possibility of good dissolution rate as indicated by Sanphui et al.[33]

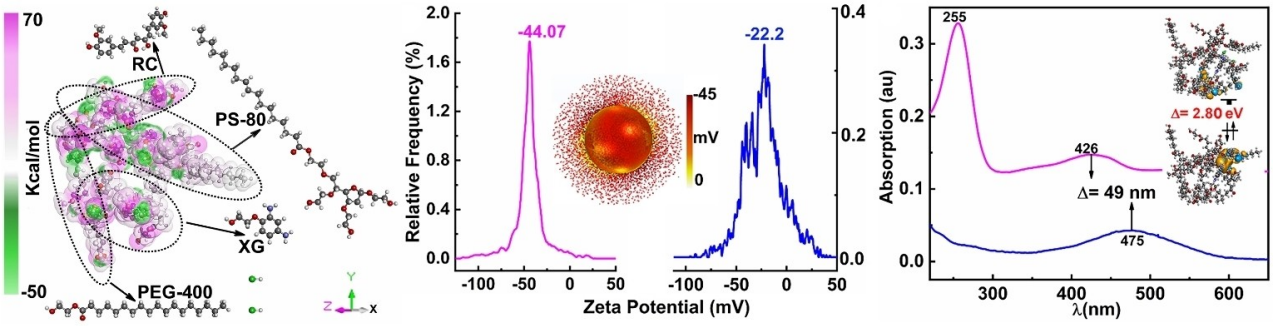

Figure 3. (A) Electrostatic potential (ESP) mapped van der Waals (vdW) surface of DFT-simulated CurNP complex. The map reveals molecular interaction sites of XG, PEG-400, PS-80 with RC in parrot green (− ve energy values) and magenta colour (+ ve energy values). There is a substantial portion of vdW, which has large negative value of ESP (−50 to −30 kcal mol^{-1}, in parrot green colour), which is attributed to the carbonyl group and oxygen atoms of the carboxyl and hydroxyl groups. A tiny part of the vdW surface has very low ESP (−10 to +10 kcal mol^{-1}) that stems from C–H coordination (in pale white colour). The ESP global minima and maxima on the simulated CurNPs' surface are −49.83 and +69.92 kcal mol^{-1}, respectively. (B) Zeta potential of RC and CurNP (blue and magenta colour lines respectively), demonstrating the stability of CurNP. The inset shows COMSOL Multiphysics (Ver. 5.4) simulated surface charge density around CurNP. (C) Absorption spectra of RC and CurNP (blue and magenta colour lines, respectively) with CurNP showing a blue shift. The insets shows the HOMO–LUMO molecular energy gap obtained from structural and density functional theory simulation calculations using Materials Studio Software Suite 2017 (Accelrys) for CurNP (top right).

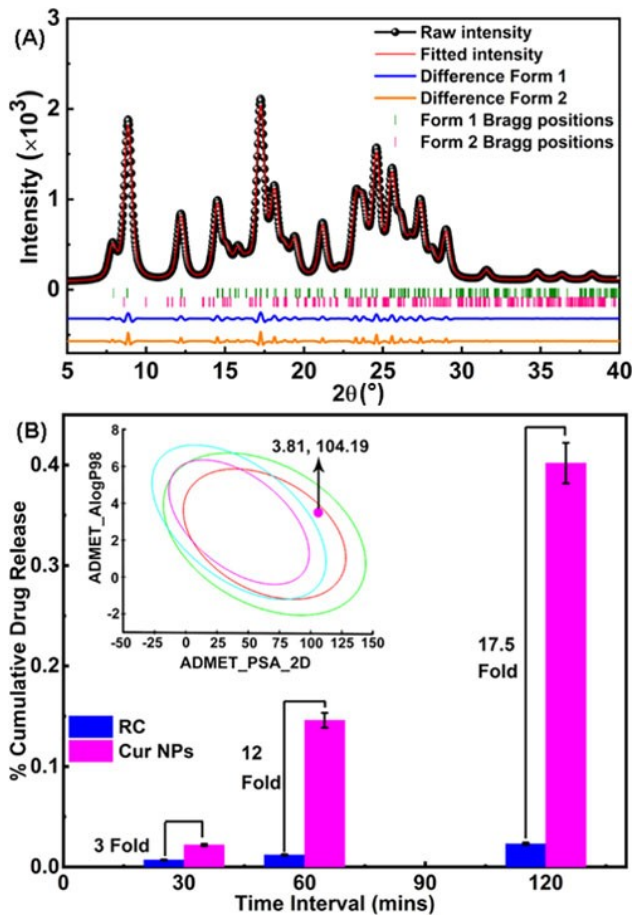

Figure 4. (A) Rietveld-refined XRD patterns of CurNP showing Bragg peaks for Form-1 and Form-2. (B) Comparative Permeation study of RC (blue line) and CurNP (magenta line) over a time interval of 120 min. At 120 min, CurNP shows 17.5-fold higher permeation than RC as demonstrated by in vitro Franz diffusion method. Drug absorption prediction (inset) for CurNP [Discovery Studio 2.1 (Accelrys)]. Two-dimensional polar surface area (PSA 2D) for CurNP is plotted against their calculated atom-type partition coefficient (ALogP98), both an ADMET descriptor.

After confirmation of good dispersion stability and dissolution rate of CurNP, the in vitro intestinal permeation potentials of RC and CurNP were evaluated (representative Figures 1D and 1E). At all the test time intervals, CurNP demonstrated enhanced permeation compared to RC and at 120 min duration CurNP had 17.5-fold better permeation than RC (Figure 4B). The permeation results were further validated with in silico drug absorption prediction using ADMET predictors (Discovery Studio 2.1).[34]

In the ADMET predictor analysis, PSA 2D is an indicator of good human intestinal absorption and AlogP98 for molecular lipophilicity.[35] The relation between AlogP98 and PSA_2D with 95% and 99% confidence ellipses suggests that the molecule will be well absorbed 95 and 99 out of 100 times, respectively.[35a] From an ADMET analysis of CurNP, we observed the PSA_2D value to be 104.19 and AlogP98 as 3.81 which falls well within the 95% confidence ellipse (Figure 4B inset; Figure S8, Supporting Information). The above in silico analysis confirms enhanced permeation observed in experimental studies.

Conclusion

In conclusion, a unique approach has been demonstrated for the room temperature telescoping synthesis of XG-stabilised, PEG-conjugated CurNP complex. The confirmation of CurNP formation, its enhanced dispersion stability, higher dissolution rate along with multi-fold permeation potential will unleash the therapeutic potential of CurNP.

Experimental Section

DFT Simulation

DFT calculations were carried out using the Discovery studio 2017 (Accelrys, San Diego, CA, USA). The RC molecular structure were obtained from PubChem (ID: 969516). The molecular structures of RC, PS-80, XG & PEG-400 were geometry optimized using Dmol3 server, via the use of the Double Numerical Plus Polarization basis set and B3LYP function. The calculations were performed with fine quality grid. The interactions of above geometry optimized molecules were simulated with Conductor-like Screening Model (COSMO) considering water as a solvent and above-mentioned calculation functions sets. During DFT calculations binding energy, binding site, HOMO-LUMO molecular orbitals, electrostatic surface potential of individual and resultant molecule was simulated.[36] The occupied and unoccupied volumes within CurNP were evaluated by constructing a supercell of dimension $5\times5\times5$ followed by Connolly surface construction with a fine grid resolution (0.25 Å) and a Connolly radius set to 1.0 Å. We determined binding energy of interactions of RC with other reactants. The calculation shows that RC interacts at $\Delta E \approx 63.4\ \text{kcal mol}^{-1}$ with other reactants (Figure S3(B)). It is interesting to note that simulated single CurNP unit contain occupied volume 3709.56 $Å^3$, unoccupied volume 6696.89 $Å^3$ with large surface area 2908.42 $Å^2$ (Figure S3(C)).

Acknowledgements

This work was supported by the Plant Cell Project 2022P4 from the Plant Cell Research Institute of BIO-FD&C Co.; Ltd.; South Korea. We would like to express our gratitude to Symbiosis Centre for Research and innovation (SCRI) for providing senior research fellowship to Prem Pandey.

Conflict of Interest

The authors declare no conflict of interest.

Data Availability Statement

The data that support the findings of this study are available from the corresponding author upon reasonable request.

Keywords: DFT simulation · nanocurcumin · PEG conjugation · permeation potential · telescoping synthesis

[1] a) B. Farhood, K. Mortezaee, N. H. Goradel, N. Khanlarkhani, E. Salehi, M. S. Nashtaei, M. Najafi, A. Sahebkar, *J. Cell. Physiol.* **2019**, *234*, 5728–5740; b) J. W. Morzycki, L. Rárová, J. Grúz, T. Sawczuk, U. Kiełczewska, L. Siergiejczyk, A. Wojtkielewicz, *ChemistryOpen* **2016**, *5*, 339–350.
[2] A. Theppawong, T. Van de Walle, C. Grootaert, K. Van Hecke, N. Catry, T. Desmet, J. Van Camp, M. D'Hooghe, *ChemistryOpen* **2019**, *8*, 236–247.
[3] Y. Zhang, L. Li, J. Zhang, *Basic Clin. Pharmacol. Toxicol.* **2020**, *127*, 243–253.
[4] S. Qin, L. Huang, J. Gong, S. Shen, J. Huang, H. Ren, H. Hu, *Nutr. J.* **2017**, *16*, 68.
[5] a) S. Kundur, A. Prayag, P. Selvakumar, H. Nguyen, L. McKee, C. Cruz, A. Srinivasan, S. Shoyele, A. Lakshmikuttyamma, *J. Cell. Physiol.* **2019**, *234*, 11103–11118; b) A. Giordano, G. Tommonaro, *Nutrients* **2019**, *11*, 2376; c) K. K. Laali, A. T. Zwarycz, N. Beck, G. L. Borosky, M. Nukaya, G. D. Kennedy, *ChemistryOpen* **2020**, *9*, 822–834.
[6] H. Wang, H. Sui, Y. Zheng, Y. Jiang, Y. Shi, J. Liang, L. Zhao, *Nanoscale* **2019**, *11*, 7481–7496.
[7] J. Zheng, J. Cheng, S. Zheng, Q. Feng, X. Xiao, *Front. Pharmacol.* **2018**, *9*, 472.
[8] a) P. Anand, A. B. Kunnumakkara, R. A. Newman, B. B. Aggarwal, *Mol. Pharmaceutics* **2007**, *4*, 807–818; b) Y. Lu, M. Lin, J. Zong, L. Zong, Z. Zhao, S. Wang, Z. Zhang, M. Han, *Food Sci. Nutr.* **2020**, *8*, 6415–6425.
[9] M. Dei Cas, R. Ghidoni, *Nutrients* **2019**, *11*, 2147.
[10] a) S. Flory, N. Sus, K. Haas, S. Jehle, E. Kienhöfer, R. Waehler, G. Adler, S. Venturelli, J. Frank, *Mol. Nutr. Food Res.* **2021**, *65*, 2100613; b) C. H. N. Barros, H. Devlin, D. W. Hiebner, S. Vitale, L. Quinn, E. Casey, *Nanoscale Adv.* **2020**, *2*, 1694–1708.
[11] a) L. Li, W. Wan, W. Cheng, G. Liu, L. Han, *Int. J. Food Sci. Technol.* **2019**, *54*, 2502–2510; b) T. Gupta, J. Singh, S. Kaur, S. Sandhu, G. Singh, I. P. Kaur, *Front. Bioeng. Biotechnol.* **2020**, *8*, 879.
[12] a) A. Catalán-Latorre, M. Pleguezuelos-Villa, I. Castangia, M. L. Manca, C. Caddeo, A. Nácher, O. Díez-Sales, J. E. Peris, R. Pons, E. Escribano-Ferrer, A. M. Fadda, M. Manconi, *Nanoscale* **2018**, *10*, 1957–1969; b) A. Moquin, R. Hanna, T. Liang, H. Erguven, E. R. Gran, B. A. Arndtsen, D. Maysinger, A. Kakkar, *Chem. Commun.* **2019**, *55*, 9829–9832.
[13] Z. Li, M. Shi, N. Li, R. Xu, *Front. Chem.* **2020**, *8*, 589957.
[14] J. Karlsson, H. J. Vaughan, J. J. Green, *Annu. Rev. Chem. Biomol. Eng.* **2018**, *9*, 105–127.
[15] S. Chen, Y. Han, J. Huang, L. Dai, J. Du, D. J. McClements, L. Mao, J. Liu, Y. Gao, *ACS Appl. Mater. Interfaces* **2019**, *11*, 16922–16933.
[16] S. Dey, K. Sreenivasan, *Carbohydr. Polym.* **2014**, *99*, 499–507.
[17] Y. Lee, D. H. Thompson, *Wiley Interdiscip. Rev.: Nanomed. Nanobiotechnol.* **2017**, *9*, e1450.
[18] T. T. Hoang Thi, E. H. Pilkington, D. H. Nguyen, J. S. Lee, K. D. Park, N. P. Truong, *Polymer* **2020**, *12*, 298.
[19] A. Wang, Y. Li, X. Yang, M. Bao, H. Cheng, *Mar. Pollut. Bull.* **2017**, *118*, 275–280.
[20] S. C. Gupta, S. Prasad, J. H. Kim, S. Patchva, L. J. Webb, I. K. Priyadarsini, B. B. Aggarwal, *Nat. Prod. Rep.* **2011**, *28*, 1937–1955.
[21] S. Manimaran, K. SambathKumar, R. Gayathri, K. Raja, N. Rajkamal, M. Venkatachalapathy, G. Ravichandran, C. Lourdu EdisonRaj, *Nat. Prod. Bioprospect.* **2018**, *8*, 369–390.
[22] X. Chen, L. Zou, J. Niu, W. Liu, S.-F. Peng, C.-M. Liu, *Molecules* **2015**, *20*, 14293–14311.
[23] a) S. Faria, C. L. de Oliveira Petkowicz, S. A. L. de Morais, M. G. H. Terrones, M. M. de Resende, F. P. de França, V. L. Cardoso, *Carbohydr. Polym.* **2011**, *86*, 469–476; b) A. Reddy Polu, R. Kumar, *J. Chem.* **2011**, *8*, 347–353.
[24] A. V. Singh, A. Kayal, A. Malik, R. S. Maharjan, P. Dietrich, A. Thissen, K. Siewert, C. Curato, K. Pande, D. Prahlad, N. Kulkarni, P. Laux, A. Luch, *Langmuir* **2022**, *38*, 7976–7988.
[25] X. An, Y. Kang, G. J. C. P. Li, *Chem. Phys.* **2019**, *520*, 100–107.
[26] S. R. Gadre, C. H. Suresh, N. Mohan, *Molecules* **2021**, *26*, 3289.
[27] B. C. Smith, *Fundamentals of Fourier transform infrared spectroscopy*, CRC press, **2011**.
[28] S. S. Pingale, S. R. Gadre, *Chem. Phys. Lett.* **2001**, *340*, 604–610.
[29] a) S. Samimi, N. Maghsoudnia, R. B. Eftekhari, F. Dorkoosh, in *Characterization and Biology of Nanomaterials for Drug Delivery* (Eds.: S. S. Mohapatra, S. Ranjan, N. Dasgupta, R. K. Mishra, S. Thomas), Elsevier, **2019**, pp. 47–76; b) A. Karthikeyan, N. Senthil, T. Min, *Front. Pharmacol.* **2020**, *11*, 487.
[30] D. H. Hanna, G. R. Saad, *RSC Adv.* **2020**, *10*, 20724–20737.
[31] J. Nayak, R. Mythili, M. Vijayalakshmi, S. N. Sahu, *Phys. E (Amsterdam, Neth.)* **2004**, *24*, 227–233.
[32] K. Kandori, K. Kon-no, A. Kitahara, *Bull. Chem. Soc. Jpn.* **1984**, *57*, 3419–3425.
[33] P. Sanphui, N. R. Goud, U. B. R. Khandavilli, S. Bhanoth, A. Nangia, *Chem. Commun.* **2011**, *47*, 5013–5015.
[34] R. S. Maharjan, A. V. Singh, J. Hanif, D. Rosenkranz, R. Haidar, A. Shelar, S. P. Singh, A. Dey, R. Patil, P. Zamboni, P. Laux, A. Luch, *ACS Omega* **2022**, *7*, 13985–13997.
[35] a) W. J. Egan, K. M. Merz, J. J. Baldwin, *J. Med. Chem.* **2000**, *43*, 3867–3877; b) M. E. Soliman, A. T. Adewumi, O. B. Akawa, T. I. Subair, F. O. Okunlola, O. E. Akinsuku, S. Khan, in *AAPS PharmSciTech, Vol. 23*, **2022**, p. 86.
[36] A. V. Singh, M. H. D. Ansari, D. Rosenkranz, R. S. Maharjan, F. L. Kriegel, K. Gandhi, A. Kanase, R. Singh, P. Laux, A. Luch, *Adv. Healthcare Mater.* **2020**, *9*, 1901862.

Manuscript received: September 14, 2022
Revised manuscript received: December 1, 2022